The Journal of Engineering Geology, Vol.11, No.3, December, 2001.pp.255-267

화강암반내 단층지역에 위치한 지하 방사성폐기물 처분장 인접지역에서의 열-수리-역학적 연성거동 비교 연구

A comparison study on coupled thermal, hydraulic, and mechanical interactions associated with an underground radwaste repository within a faulted granitic rock mass

김 진 웅(Jhinwung Kim) 한국원자력연구소
배 대 석(Daeseok Bae) 한국원자력연구소
강 철 형(Chul-Hyung Kang) 한국원자력연구소

요약 / ABSTRACT

지하 500 m의 화강암반내 단층지역에 위치한 지하 방사성폐기물 처분장 인접지역에서의 열, 수리, 및 역학적 연성거동을 비교하고 분석하였다. 해석에는 2차원 해석코드인 UDEC을 사용하였다.

해석모델은 화강암반, 처분공내의 압축 벤토나이트로 둘러싸인 PWR 사용후 핵연료 처분용기, 및 처분 동굴내에 채워진 혼합 벤토나이트를 포함한다.

수리-역학적, 열-역학적, 및 열-수리-역학적 연성거동을 비교 및 분석하였다. PWR 사용후 핵연료내의 방사성 물질로부터 나오는 시간의존 방사성 붕괴열이 처분장 및 인접지역에 미치는 영향을 분석하였다. 수리해석에는 steady state flow 알고리즘을 사용하였다.

주요어: 상호작용 거동, 열-수리-역학적 상호작용, 방사성폐기물 처분장, 화강암, 단층, 동굴, UDEC, 붕괴열, steady state flow 알고리즘

A comparison study is performed to understand the coupling behavior of the thermal, hydraulic, and mechanical interactions in the vicinity of an underground radwaste repository, assumed to be located at a depth of 500 m, within a granitic rock mass with a 58° dipping fault passing through the roof-wall intersection of the repository cavern. The two dimensional universal distinct element code, UDEC is used for the analysis.

The model includes a granitic rock mass, a canister with PWR spent fuels surrounded by the compacted bentonite inside a deposition hole, and the mixed bentonite backfilled in the rest of the

space within a repository cavern.

The coupling behavior of hydromechanical, thermomechanical, and thermohydromechanical interaction has been studied and compared. The effect of the time-dependent decaying heat, from the radioactive materials in PWR spent fuels, on the repository and its surroundings has been studied. A steady state flow algorithm is used for the hydraulic analysis.

Key words: coupling behavior, thermohydromechanical interaction, radwaste repository, granite, fault, cavern, UDEC, decaying heat, steady state flow

1. Introduction

The assessment of the coupling effects of thermal, hydraulic, and mechanical interactions in the vicinity of a very deep underground radwaste repository in a granitic rock mass with discontinuities is an important part of the design and safety evaluation of the disposal system.

The state of the art studies on the various coupled processes for rock joints have been summarized by Tsang(1990). The most common distinct element method considers the fractured medium as an assembly of blocks(Barton,1988; Fairhurst et al,1987). For coupled thermal and mechanical behavior, the distinct element method has been used to analyze the behavior of the fractured rock masses for a radioactive waste repository(Shen et al,1990). For coupled hydraulic and thermal behavior, the effect of increasing temperature, due to the decay heat of the waste, on the ground water flow around a repository has been studied by many researchers (Hart,1981;Noorishad et al,1984). For coupled hydraulic, mechanical, and thermal behavior, Hart(1981) presented a model which fully describes coupled behavior in nonlinear porous geological systems, and the model is solved by an explicit finite difference method. Noorishad et al(1984) applied a finite element method with joint elements to fully couple the behavior for a saturated fractured rock mass. Ohnishi et al (1985) developed a finite element code to handle the problems of coupled hydraulic, thermal, and mechanical behavior of a saturated- unsaturated geological medium.

The objective of the present study is to understand the coupling behavior of hydromechanical, thermomechanical, and thermohydromechanical interactions in the vicinity of a 500 m deep underground radwaste repository in a granitic rock mass with a 58° dipping fault intersecting the roof of the repository.

2. Numerical model

The repository has the layout of multiple caverns in parallel with a cavern spacing of 40 m. Each cavern is 250 m long, 6 m wide, and 7 m high from the floor to the crown of the cavern. The vertical deposition holes are located beneath the cavern floor along the centerline of the cavern at a pitch of 6 m.

Four assemblies of PWR spent fuels cooled for 40 years are emplaced and fixed with a cast iron insert between the fuel assemblies and the hollow cylindrical canister. And then, compacted bentonite fills the area between the canister and the surrounding rock mass, and backfill material fills the inside the cavern(Fig.1). The radioactive materials in PWR spent fuels generate decay heat. The decay heat generated, H(T) in w/tHM(watt/metric ton of heavy metal) is defined as follows(Kang et al,2000):

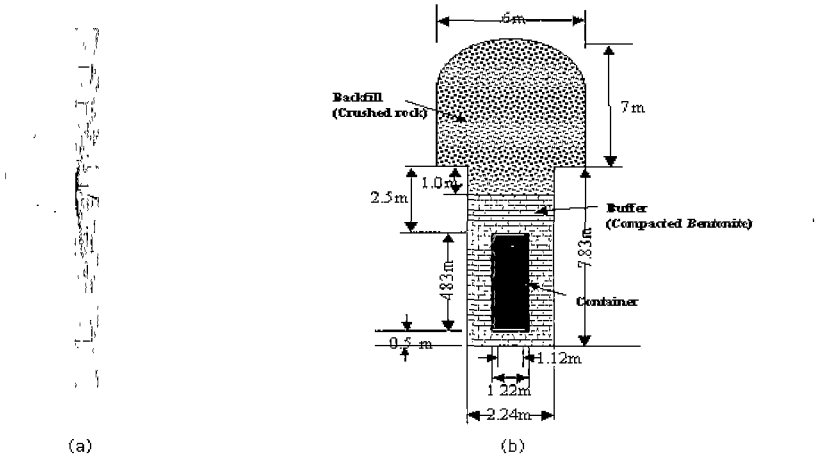

Fig. 1 The (a)numerical model and (b)a cavern and a deposition hole with a canister

$$H=2201169e^{-5.205T}+1693.22e^{-0.018T}+124.7e^{-0.00058T}+19.134e^{-0.000042T}+1.429e^{-0.000001T} \quad (1)$$

where, T is the time after discharging PWR spent fuels, $0 \le T \le 10^6$ years

In order to do the two dimensional approximation using UDEC code, this discrete waste location is distributed uniformly along the disposal cavern. This means that the heat generating trench is located below the cavern floor along the centerline of the disposal cavern. After the consideration of the tributary heating area of 10,000 m^2 which is equal to the area of the cavern length of 250 m multiplied by the cavern spacing of 40 m, heat flux, F, is then obtained from the equation (1),

$$F=(28.0554)e^{-(5.708E-10)t}+(4.1492)e^{-(1.839E-11)t}+(0.6486)e^{-(1.332E-12)t}+(0.04876)e^{-(3.171E-14)t} \quad (2)$$

where, t is the time after 40 years of cooling, $0 \le t \le 3.1536E13$ sec, F in w/m^2

2.1 Modeling

The model is for the simulation of the coupled behavior between thermal, hydraulic, and mechanical interactions for the long term behavior(500 years) of a radioactive waste repository.

To simplify the analysis, the symmetry in the repository layout of multiple caverns in parallel with an equal spacing has been utilized in modeling. The top and bottom horizontal boundaries are moved sufficiently far from the heat generating waste. The excavation of the cavern, waste emplacement, and buffer filling are all assumed to be instantaneous, and the initial horizontal stress is assumed to be equal to the initial vertical stress in the analysis. Groundwater flow is idealized as laminar viscous flow.

Granitic rock mass is assumed to be homogeneous and isotropic with elastoplastic behavior(Mohr-Coulomb failure criteria applied), and compacted and mixed bentonite are regarded as elastoplastic material(Drucker-Prager failure criteria applied). The material for the canister is assumed to be homogeneous, isotropic, and linearly elastic. Barton-Bandis joint constitutive model is used for the rock joints(Itasca,1996).

For the hydraulic analysis using a steady state flow algorithm, groundwater flows through the discontinuities of the rock mass. A fully coupled hydromechanical analysis is performed in which fracture conductivity is dependent on mechanical deformation of the joint aperture;

conversely, joint water pressures affect the mechanical behavior. Groundwater flow is governed by the pressure differential between adjacent domains. The cubic law for flow in a planar fracture is used in UDEC(Itasca,1996). The flow rate, q, from a domain with pressure p_1 to a domain with pressure p_2 is given by

$$q = -k_j a^3(\triangle p/l) \quad (3)$$

where k_j is a joint permeability factor whose theoretical value is $(1/12\mu)$, μ is the dynamic viscosity of the fluid, a is the contact hydraulic aperture, and l is the length assigned to the contact between domains.

$$\triangle p = p_2 - p_1 + \rho_w g(y_2 - y_1) \quad (4)$$

where ρ_w is the fluid density, g is the acceleration of gravity, and y_1, y_2 are the y-coordinates of the domain centers.

The hydraulic aperture is given by

$$a = a_o + u_n \quad (5)$$

where a_o is the joint aperture at zero normal stress, and u_n is the joint normal displacement.

For the thermal analysis, this model simulates transient heat conduction in materials and the subsequent development of thermally induced displacements and stresses. Heat transfer is modeled as isotropic conduction and heat decays exponentially with time. The thermal analysis in UDEC(Itasca,1996) provides only one-way coupling to the mechanical stress calculation through the thermal expansion coefficient and to the calculation for groundwater flow in joints through the temperature dependency of groundwater density and joint permeability. The basic equation of conductive heat transfer is Fourier's law.

$$Q_i = -k_{ij}(\partial T/\partial x_j) \quad (6)$$

where Q_i is the heat flux in the i-direction, k_{ij} is the thermal conductivity tensor, and T is the temperature. The change in temperature for any mass is as follows,

$$(\partial T/\partial t) = Q_{net}/(C_p M) \quad (7)$$

where Q_{net} is the net heat flow into mass, C_p is the specific heat, and M is the mass.

The equations (6) and (7) are the basis of the thermal version of UDEC. Temperature changes cause stress changes,

$$\triangle \sigma_{ij} = -\delta_{ij}\, 3\, K^* \alpha \triangle T \quad (8)$$

where $\triangle \sigma_{ij}$ is the change in stress ij, δ_{ij} is the Kronecker delta, K^* is K(for plane strain) and is equal to 6KG/(3K+4G) for plane stress, K is the bulk modulus, G is the shear modulus, α is the linear thermal expansion coefficient, and $\triangle T$ is the temperature change.

2.2 Initial and boundary conditions

Symmetric boundary conditions are used due to the repository layout of multiple cavern in parallel with an equal shape, length, and spacing.

The boundary conditions for this fully saturated 200 m model are fixed horizontal displacements on both sides, fixed vertical displacement at the bottom, and free at the surface. Impermeable boundary conditions are assumed on both sides and at the bottom of the model. The thermal boundary conditions are adiabatic on both sides and at the bottom. The temperature is assumed to be 20℃ at the ground surface and to increase 0.6℃ for every 20 m below the surface. Therefore, the initial temperature is 32℃ at the top and 38℃ at the bottom of the model.

2.3 Material properties

Material properties for the host granitic rock, rock fault, compacted and mixed bentonite, and canister cast iron insert are as follows(Kang et al,2000; Hokmark et al,1991; Hokmark,1990; Johansson et al,1991; SKB,1997; SKB,1997):

Table 1. Mechanical and thermal properties of granite

Parameter	Value
density	2700.0 kg/m^3
bulk modulus	40.0 GPa
shear modulus	24.0 GPa
thermal conductivity	3.2 W/mC
thermal expansion coeff.	8.3E-6 1/℃
specific heat	815.0 J/kgC
friction angle	25.0°
cohesion	16.0 MPa
dilation	8.0

Table 2. Mechanical properties of a fault

Parameter	Value
joint normal stiffness	1.6E4 GPa/m
joint shear stiffness	7.0E3 GPa/m
joint cohesion	0.1 MPa
joint dilation	0.0°
joint aperture	1.0E-2 m
joint permeability	3.0 1/(Pa*sec)
joint residual aperture	5.0E-4 m
joint length	0.1 m
joint roughness coeff.	5.0
joint comp. strength	30.0 MPa
residual angle of friction	45.0°
intact rock comp. str.	200.0 MPa

Table 3. Mechanical and thermal properties of compacted bentonite

Parameter	Value
density	2100.0 kg/m^3
bulk modulus	3.5 GPa
shear modulus	0.75 GPa
thermal conductivity	1.2 W/mC
thermal expansion coeff.	0.0 1/℃
specific heat	1000.0 J/kgC

Table 4. Mechanical and thermal properties of mixed-bentonite

Parameter	Value
density	2100.0 kg/m^3
bulk modulus	3.33 GPa
shear modulus	1.54 GPa
thermal conductivity	2.0 W/mC
thermal expansion coeff.	8.3E-6 1/℃
specific heat	800.0 J/kgC

Table 5. Mechanical and thermal properties of canister cast iron insert

Parameter	Value
density	8000.0 kg/m^3
bulk modulus	167.0 GPa
shear modulus	77.0 GPa
thermal conductivity	15.2 W/mC
thermal expansion coeff.	8.2E-6 1/℃
specific heat	504.0 J/kgC

3. Results

Three different cases of coupled behavior between thermal, hydraulic, and mechanical interactions have been studied and compared. The model used here for comparison purposes is a 200 m model with a 58° dipping fault intersecting the cavern roof-wall intersection. The first case is the hydromechanical(HM) model using a steady state flow algorithm. The second case is the thermomechanical(TM) model in a dry condition without groundwater for a period of 500 years after the emplacement of the canister and filling with buffer materials. The last case is the thermohydromechanical(THM) model fully saturated using a steady state flow algorithm for a period of 500 years after the emplacement of the canister and filling with buffer materials.

3.1 Initial stage

At the initial stage, the loads acting on the models are mainly the weight of the granitic rock mass either saturated, or in a dry condition. The initial ground temperature of 32℃ on the top of the model and of 0.6℃ increase for every 20 m below the top boundary is applied on the TM and THM models. The initial vertical and horizontal stress distributions are shown in Figs. 2(a) and (b), respectively. The maximum principal stresses occur at the top of the models and are -10.68 MPa on the HM model and -10.67 MPa on the TM and THM models. The minimum principal stresses occur at the bottom of the models and are -15.76 MPa on the HM model and -16.06 MPa on the TM and THM models.

3.2 After instantaneous excavation

After the instantaneous excavation, the stresses are concentrated around the cavern. The highest principal stresses occur at the locations just above the top of the cavern wall and are -20.88 MPa on the HM model, -24.92 MPa on the TM model, and -20.88 MPa on the THM model. The maximum displacements occur at the cavern floor-deposition hole intersection in the direction toward the center of the cavern horizontally and are 1.093 mm on the HM model, 1.632 mm on the TM model, and 1.095 mm on the THM model. The maximum shear displacements are 0.835 mm, 1.073 mm, and 0.835 mm on the HM, TM, and THM models, in that order, at the location on the rock close to the center of the canister.

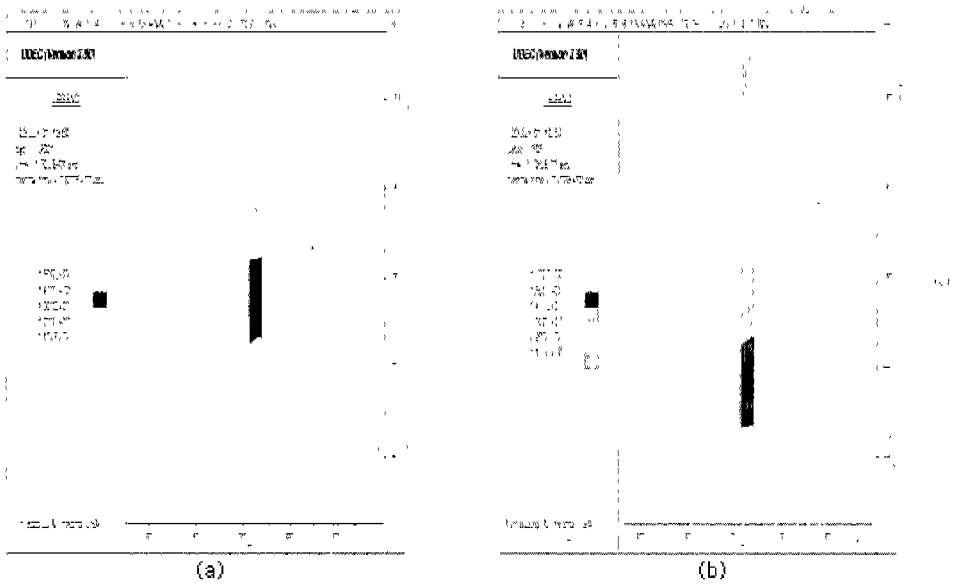

Fig. 2 The (a)vertical and (b)horizontal stress distributions on the 200m model at the initial stage

Results along the fault from the analysis after instantaneous excavation are summarized in Table 6. The normal stresses are higher, while shear stresses are lower on the TM model than on the HM and THM models. The hydraulic aperture distribution is the same in all three models.

3.3 After waste emplacement and buffer filling

The waste emplacement, and compacted and mixed bentonite filling are assumed to be instantaneous. After waste emplacement and buffer filling, the highest principal stresses occur at the locations just above the top of the cavern wall and are in turn -24.0 MPa, -24.91 MPa, and -24.02 MPa on the HM, TM, and THM models. The maximum displacements at the locations of the cavern floor-deposition hole intersection are 1.413 mm, 1.631 mm, and 1.429 mm on the HM, TM, and THM models, in that order, in the horizontal direction toward the center of the cavern. The maximum shear displacements at the locations on the rock close to the center of the canister are 0.912 mm, 1.072 mm, and 0.913 mm on the HM, TM, and THM models, in that order.

Results along the fault from the analysis after buffer filling are in Table 7. The normal stresses after buffer filling are lower, while shear stresses after buffer filling are higher than the normal and shear stresses after excavation. The hydraulic apertures along the fault become smaller after buffer filling.

3.4 Long term behavior after waste emplacement

The long term structural behavior of the coupled thermohydromechanical interaction, for a period of 500 years after waste emplacement, on a 200 m fully saturated model with a 58℃ dipping fault intersecting the cavern roof is shown in

Table 6. Results along the fault from the analysis after excavation

Results\Models	HM	TM	THM
hyd. aperture, m	2.194E-4~3.252E-4	2.194E-4~3.252E-4	2.194E-4~3.252E-4
normal stress, MPa	5.341~17.59	8.661~27.43	5.355~18.07
shear stress, Pa	-4.049E5~1.214E5	-8.558E4~2.045E5	-4.392E5~1.233E5
normal displ.,m	0	0	0
shear displ., m	-3.531E-4~2.299E-5	-4.557E-4~3.86E-5	-3.534E-4~2.261E-5
domain press., MPa	4.427~4.638	0	4.427~4.638

Table 7. Results along the fault from the analysis after buffer filling

Results\Models	HM	TM	THM
hyd. aperture, m	1.097E-4~2.194E 4	1.097E-4~2.194E-4	1.097E-4~2.194E-4
normal stress, MPa	4.644~11.69	8.667~16.54	4.617~11.69
shear stress, Pa	-9.606E5~1.25E5	-8.665E4~1.027E6	-9.302E5~1.217E5
normal displ., m	0	0	0
shear displ., m	-3.804E-4~3.897E-5	-4.554E-4~3.906E-5	-3.8E-4~3.982E-5
domain press., MPa	4.427~4.638	0	4.427~4.638

Fig. 3. Temperature histories are shown in Fig. 3(a). The top, middle, and bottom history curves are in turn for the locations of the center of the canister which is the center of the heat source, of 0.61 m away horizontally from the canister center where the canister faces with the compacted bentonite, and of 1.12 m away horizontally from the canister center where the bentonite faces with the rock. The curves show maximum temperatures of 86℃~91℃ after 41~54 years, and then decay fastly down to 74℃~75℃ after 500 years from waste emplacement.

Displacement histories are shown in Fig. 3(b). The five history curves from the top are the displacements for the locations of the cavern roof-wall intersection, cavern floor center, cavern crown, cavern floor-deposition hole intersection, and cavern floor-wall intersection. The displacement history of cavern crown shows fast convergence approximately after the first 100 years. The rest of the history curves show fairly constant displacements.

Normal stress histories are shown in Fig. 3(c). The three history curves from the top are the normal stresses for the locations near the cavern roof-wall intersection, cavern floor center, and mid-point on the cavern roof. The normal stress near the cavern roof-wall intersection shows fast convergence approximately after the first 100 years. The other two history curves show fairly constant normal stresses during the period of 500 years.

Shear stress histories are shown in Fig. 3(d). The three history curves from the top are for

(a)

(b)

(c)

(d)

Fig. 3 The (a)temperature histories, (b)displacement, (c)normal strss, and (d)shear stress histories of the points in the vicinity of the cavern after 500 years of waste emplacement

the locations near a mid-point on the cavern roof, cavern floor-wall intersection, and cavern roof-wall intersection. The shear stress near the cavern roof-wall intersection increases fastly in magnitude for the first 100 years after waste emplacement, and then decreases slowly. The rest of the history curves show constant shear stresses during the period of 500 years.

The temperature distribution on the 200 m model and its enlarged view in the vicinity of the repository after 500 years of waste emplacement are shown in Figs. 4(a) and (b).

A comparison study is performed to understand the coupled HM, TM, THM interactions in the vicinity of a repository for a period of 100 years after waste emplacement, because the history curves for stresses and displacements show maximum responses approximately after 100 years from waste emplacement, even though the temperatures reach maximum values in the vicinity of the repository after approximately 50 years from waste emplacement as shown in Fig. 3(a).

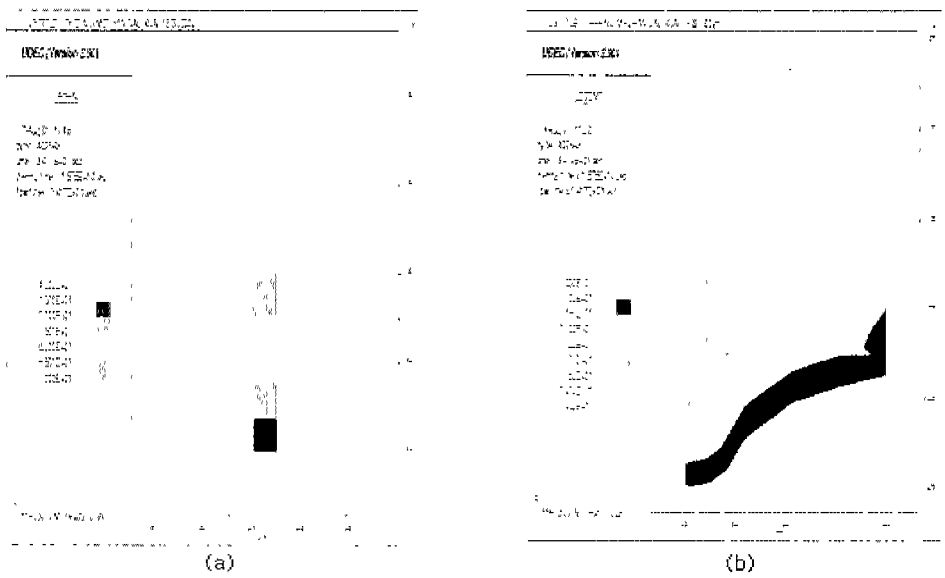

Fig. 4 The (a)temperature distriution on the model and (b)its enlarged view in the vicinity of the repository after 500 years from waste emplacement

Maximum and minimum principal stresses in the vicinity of the repository are summarized in Table 8 for each HM, TM, THM models. The stresses near wall-roof intersection, at the center of backfill, below the cavern floor, and below the deposition hole are slightly higher in the THM model, while the stresses near the cavern wall and near the wall-floor intersection are slightly higher in the TM model. The stresses in the HM model are much lower than the stresses in the TM and THM models.

Displacements at the locations around the repository are summarized in Table 9 for each HM, TM, and THM models. The displacements generally are larger in the TM model than in the THM model, and they are in the range of 3.256cm~4.084cm. But the differences between the two models are very small and are less than 0.34%. The displacements are much smaller in the HM model than in the rest of the models.

Shear displacements on the 58° dipping fault after 100 years of waste emplacement in Table 10 show much larger values in the TM and THM models than in the HM model. The shear displacements in the THM model are smaller at the left end of the fault close to the cavern and larger at the right end of the fault away from the cavern than the shear displacements in the TM model.

Hydraulic apertures and hydraulic permeabilities on the 58° dipping fault after 100 years of waste emplacement, as shown in Table 11, are 2.194E-4 m and 4.01E-5 cm^2, respectively both at the left end of the fault close to the cavern

Table 8. Maximum and minimum principal stresses after 100 years of waste emplacement (unit: Pa)

Locations\Models	HM	TM	THM
near wall-roof intersection	-2.4E7 -1.427E7	-6.771E7 -7.095E6	-6.777E7 -7.153E6
at the center of backfill	-4.367E5 -3.665E5	-4.366E6 -2.272E6	-4.806E6 -2.619E6
near the cavern wall	-2.159E7 -1.093E7	-3.764E7 -1.553E7	-3.604E7 -1.573E7
near the wall-floor intersection	-1.868E7 -2.828E6	-2.001E7 -1.071E7	-1.97E7 -1.257E7
below the cavern floor	-1.207E7 -6.664E6	-3.22E7 -9.625E6	-3.301E7 -9.688E6
below the deposition hole	-2.395E7 -1.606E7	-8.987E7 -2.408E7	-9.168E7 -2.437E7

Table 9. Displacements after 100 years of waste emplacement (unit: m)

Locations\Models	HM	TM	THM
cavern crown	8.755E-4	4.084E-2	4.079E-2
mid-point on cavern roof	9.23E-4	4.029E-2	4.024E-2
roof-wall intersection	1.0E-3	3.825E-2	3.812E-2
wall-floor intersection	1.077E-3	3.532E-2	3.535E-2
deposition hole-floor intersection	1.413E-3	3.557E-2	3.559E-2
bottom end of the fault	4.687E-5	3.503E-2	3.512E-2
a point on the rock horizontally connecting canister center	1.257E-3	3.256E-2	3.256E-2

Table 10. Shear displacements on the fault after 100 years of waste emplacement

(unit: m)

Locations\Models	HM	TM	THM
left end close to cavern	3.803E-4	2.081E-4	9.684E-5
right end away from cavern	3.906E-5	1.881E-3	2.371E-3

and at the right end of the fault away from the cavern in the HM and THM models.

The groundwater flow rates and velocities on the 58° dipping fault after 100 years of waste emplacement in Table 12 are larger at the right end of the fault away from the cavern in both HM and THM models.

Table 11. Hydraulic aperture and hydraulic permeability on the fault after 100 years of waste emplacement

Locations\Results	HM		TM		THM	
	hyd. aper.,m	hyd. perm.,cm^2	hyd. aper.,m	hyd. perm.,cm^2	hyd. aper.,m	hyd. perm.,cm^2
left end close to cavern	2.194E-4	4.01E-5	-	-	2.194E-4	4.01E-5
right end away from cavern	2.194E-4	4.01E-5	-	-	2.194E-4	4.01E-5

Table 12. Groundwater flow rate, velocity, and domain pressure on the fault after 100 years of waste emplacement

Locations\Models	HM			THM		
	flow rate m^3/sec	flow vel. m/sec	domain p. Pa	flow rate m^3/sec	flow vel. m/sec	domain p. Pa
left end close to cavern	4.477E-12	2.041E-8	4.627E6	2.728E-12	1.243E-8	4.612E6
right end away from cavern	6.176E-12	2.815E-8	4.460E6	1.146E-11	5.222E-8	4.470E6

4. Conclusion

Three different cases of coupled behavior in the vicinity of a 500 m deep underground repository within a granitic rock mass with a 58° dipping fault passing through the cavern roof have been studied and compared. They are the HM model using a steady state flow algorithm, the TM model in a dry condition, and the THM model fully saturated for a period of 500 years after the emplacement of heat generating radioactive wastes and filling with buffer materials.

For three different cases, the results from the initial state of stress analysis do not show much difference. After the excavation the maximum principal stress just above the cavern wall in the TM model is -24.92 MPa which is 19% higher than that in the HM and THM models. The maximum displacement at the cavern floor-deposition hole intersection in the TM model is 1.632 mm which is 49% larger than that in the HM and THM models. But the magnitude of these stresses and displacements are not significant. The stresses and displacements just after waste emplacement and buffer filling also do not show much difference in all three models.

For the long term thermohydromechanical behavior for a period of 500 years after heat generating waste emplacement, temperature histories along the horizontal line connecting the center of the heat source show that the maximum temperatures are 86℃~91℃ after 41~54 years, and then decays fastly down to 74℃~75℃ after 500 years from waste emplacement.

The normal and shear stress histories show that the normal and shear stresses near the cavern roof-wall intersection increase fastly for the first 100 years, and then change slowly for the rest of the period of 500 years.

Finally a comparison study is performed to understand the coupled HM, TM, and THM interactions in the vicinity of a repository after a period of 100 years from the emplacement of heat generating wastes and buffer filling.

In general, the stresses at the locations in the vicinity of the repository are higher in the THM model and they are in the range of -7 MPa~ -92 MPa on the rock mass and of +4.05 MPa~ -7.72 MPa on the buffer filling. The displacements, on the other hand, are larger in the TM model and they are in the range of 3.3 cm~4.1 cm. But the differences in stresses and displacements between the TM and THM models are not very significant. The stresses and displacements are much smaller in the HM model than in the TM and THM models.

The hydraulic apertures and hydraulic permeabilities on the fault after 100 years of waste emplacement show the same results in the HM and THM models. The groundwater flow rates and velocities on the fault are larger at the right end of the fault away from the cavern in both HM and THM models. This is due to the domain pressure differences along the line of the fault as shown in equation (3). The different magnitudes of flow rates in the HM and THM models are due to the fact that the flow rate is a function of the dynamic viscosity of the groundwater. The groundwater dynamic viscosity is a function of the water density whose values vary upon the surrounding temperature conditions.

In summary, for the design and safety evaluation of the disposal system, hydromechanical and thermomechanical analyses may be used as a start and rough estimation, but thermohydromechanical analysis is recommended to be used for the final design and safety evaluation of the disposal system.

Acknowledgement

The present study is financially supported by the National Long Term Nuclear R&D Fund from the Ministry of Science and Technology.

References

1. Tsang, C. F., 1990, Coupling behavior of rock joints, in Rock Joints(edited by N. Barton and O. Stephansson)
2. Barton, N., P. Chryssanthakis, and K. Monsen, 1988, Validation of MUDEC against Colorado school of mines block test data, SKB Technical Report, 88-14
3. Fairhurst, C. and R. D. Hart, 1987, Verification and validation of coupled mechanical/water flow effects in rock masses-some possibilities and limitations, Proc. GEOVAL-87 Symp., Stockholm
4. Shen, B. and O. Stephansson, 1990, Rock mass response to glaciation and thermal loading from nuclear waste, Pro. GEOVAL-90 Symp., Stockholm
5. Hart, R. D., 1981, A fully coupled thermal-mechanical fluid flow model for nonlinear geologic system, PhD. Thesis, Univ. of Minn., Minnesota
6. Noorishad, J., C. F. Tsang, and P. A. Witherspoon, 1984, Coupled thermal-hydraulic-mechanical phenomena in saturated fractured porous rocks-numerical approach, J. Geophy. Res. 89
7. Ohnishi, Y., H. Shibata, and A. Kobayashi, 1985, Development of finite element code for the analysis of coupled thermo-hydro-mechanical behaviors of saturated unsaturated medium, Proc. Int. Symp. Coupled processes

affecting the performance of a nuclear waste repository, Berkeley
8. Kang, Chulhyung et al, 2000, Preliminary conceptual design and performance assessment of a deep geological repository for high-level waste in the Republic of Korea, KAERI and Sandia National Lab., Rep. of Korea
9. Itasca Consulting Group, Inc., 1996, UDEC (Universal Distinct Element Code), version 3.0, Minneapolis, Minnesota
10. Hokmark, H. and I. Israelsson, 1991, Distinct element modelling of joint behavior in nearfield rock, Stripa Project 91-22, SKB
11. Hokmark, H., 1990, Distinct element method of fracture behavior in near field rock, Stripa Project 91-01, SKB
12. Johansson, E., M. Hakala, and L.J. Lorig, 1991, Rock mechanical, thermomechanical, and hydraulic behavior of the near field for spent nuclear fuel, Report YJT-91-21, TVO, Helsinki
13. SKB, 1997, Results from pre-investigations and detailed site characterizations: Summary Report, Aspo HRL-Geoscientific Evaluation 1997/2, SKB Technical Report 97-03
14. SKB, 1997, Results from pre-investigations and detailed site characterization: Summary Report, Aspo HRL-Geoscientific Evaluation 1997/2, SKB Technical Report 97-04

김진웅 (Jhinwung Kim)
Iowa State University, Civil Engineering, BS degree
University of Iowa, Structural Engineering, MS degree
Cornell University, Structural Engineering, PhD degree
Tel: 042-868-2018
E-mail: njwkim@kaeri.re.kr
At present: Principal Researcher, Korea Atomic Energy Research Institute,
Radwaste Disposal Technology Development Team

현재 : 한국원자력연구소 방사성폐기물처분 연구팀 팀장

배대석
경북대학교 문리과대학 지질학과, 이학사
충남대학교 대학원 지질학과 이학석사
충남대학교 대학원 지질학과 이학박사
Tel : 042-868-2030
E-mail : ndsbae@kaeri.re.kr
현재 : 한국원자력연구소 방사성폐기물처분연구팀 책임연구원

강칠형
서울대학교 공과대학 원자핵공학과 공학사
워싱턴대학교 대학원 원자핵공학과 공학석사
캘리포니아대학교 대학원 원자핵공학과 공학박사
Tel : 042-868-8914
E-mail : chkang@kaeri.re.kr
현재 : 한국원자력연구소 책임연구원